

Measurement and modeling of microlenses fabricated on single-photon avalanche diode arrays for fill factor recovery

Juan Mata Pavia,^{1,2,*} Martin Wolf,¹ and Edoardo Charbon^{2,3}

¹*Biomedical Optics Research Laboratory (BORL), Division of Neonatology, University Hospital Zürich (USZ), 8091 Zürich, Switzerland*

²*Quantum Architecture Group (AQUA), Ecole Polytechnique Fédérale de Lausanne (EPFL), 1015 Lausanne, Switzerland*

³*TU Delft, 2628CD Delft, Netherlands*

[*juan.matapavia@epfl.ch](mailto:juan.matapavia@epfl.ch)

Abstract: Single-photon avalanche diode (SPAD) imagers typically have a relatively low fill factor, i.e. a low proportion of the pixel's surface is light sensitive, due to in-pixel circuitry. We present a microlens array fabricated on a 128x128 single-photon avalanche diode (SPAD) imager to enhance its sensitivity. The benefit and limitations of these light concentrators are studied for low light imaging applications. We present a new simulation software that can be used to simulate microlenses' performance under different conditions and a new non-destructive contact-less method to estimate the height of the microlenses. Results of experiments and simulations are in good agreement, indicating that a gain >10 can be achieved for this particular sensor.

© 2014 Optical Society of America

OCIS codes: (030.5260) Photon counting; (040.1240) Arrays; (040.0040) Detectors; (080.0080) Geometric optics; (220.0220) Optical design and fabrication; (230.5160) Photodetectors; (240.3990) Micro-optical devices; (220.1770) Concentrators.

References and links

1. A. Rochas, M. Gosch, A. Serov, P. A. Besse, R. Popovic, T. Lasser, and R. Rigler, "First fully integrated 2-d array of single-photon detectors in standard cmos technology," *IEEE Photon. Technol. Lett.*, **15**, 963–965 (2003).
2. E. Charbon and S. Donati, "Spad sensors come of age," *Opt. Photon. News* **21**, 34–41 (2010).
3. J. Mata Pavia, E. Charbon, and M. Wolf, "3D near-infrared imaging based on a single-photon avalanche diode array sensor," *Proc. SPIE 8088, Diffuse Optical Imaging III*, 808811 (2011).
4. D.-U. Li, J. Arlt, J. Richardson, R. Walker, A. Buts, D. Stoppa, E. Charbon, and R. Henderson, "Real-time fluorescence lifetime imaging system with a 32x32 0.13 μ cmos low dark-count single-photon avalanche diode array," *Opt. Express* **18**, 10257–10269 (2010).
5. J. R. Meijlink, C. Veerappan, S. Seifert, D. Stoppa, R. Henderson, E. Charbon, and D. Schaart, "First measurement of scintillation photon arrival statistics using a high-granularity solid-state photosensor enabling time-stamping of up to 20,480 single photons," *IEEE Nucl. Sci. Symp. Med. Imag. Conf. Rec.*, pp. 2254–2257 (2011).
6. S. Mandai and E. Charbon, "Timing optimization of a h-tree based digital silicon photomultiplier," *J. Instrum.* **8**, P09016 (2013).
7. Y. Maruyama, J. Blacksberg, and E. Charbon, "A 1024x8 700ps time-gated spad line sensor for laser raman spectroscopy and libs in space and rover-based planetary exploration," *Dig. Tech. Pap. IEEE Int. Solid State Circuits Conf.*, pp. 110–111 (2013).
8. C. Veerappan, J. Richardson, R. Walker, D.-U. Li, M. W. Fishburn, Y. Maruyama, D. Stoppa, F. Borghetti, M. Gersbach, R. K. Henderson, and E. Charbon, "A 160 \times 128 single-photon image sensor with on-pixel 55ps 10b time-to-digital converter," *Dig. Tech. Pap. IEEE Int. Solid-State Circuits Conf.*, pp. 312–314 (2011).

9. L. Pancheri, N. Massari, F. Borghetti, and D. Stoppa, "A 32x32 spad pixel array with nanosecond gating and analog readout," *Proc. Intl. Image Sensor Workshop*, R40 (2011).
10. C. Niclass, C. Favi, T. Kluter, F. Monnier, and E. Charbon, "Single-photon synchronous detection," *IEEE J. Solid-State Circuits* **44**, 1977–1989 (2009).
11. M. Deguchi, T. Maruyama, F. Yamasaki, T. Hamamoto, and A. Izumi, "Microlens design using simulation program for ccd image sensor," *IEEE Trans. Consum. Electron.* **38**, 583–589 (1992).
12. S. Donati, G. Martini, and M. Norgia, "Microconcentrators to recover fill-factor in image photodetectors with pixel on-board processing circuits," *Opt. Express* **15**, 18066–18075 (2007).
13. S. Donati, G. Martini, and E. Randone, "Improving photodetector performance by means of microoptics concentrators," *J. Lightwave Technol.* **29**, 661–665 (2011).
14. C. Niclass, C. Favi, T. Kluter, M. Gersbach, and E. Charbon, "A 128x128 single-photon image sensor with column-level 10-bit time-to-digital converter array," *IEEE J. Solid-State Circuits* **43**, 2977–2989 (2008).

1. Introduction

Single-photon avalanche diodes (SPADs) are characterized by single-photon sensitivity and picosecond timing resolution, enabling to acquire time-of-flight information in addition to light intensity. Since they have become available in complementary metal-oxide-semiconductor (CMOS) technology [1], SPADs have been integrated in large arrays. SPAD arrays have been utilized in a variety of applications [2]: near-infrared imaging (NIRI) [3], fluorescence lifetime imaging microscopy (FLIM) [4], positron emission tomography (PET) [5, 6], and time-resolved Raman spectroscopy [7], to name a few. In these applications not only the light intensity but also the time of arrival the photons is measured. Traditionally, discrete detectors capable of time-resolved measurements such as photomultiplier tubes or avalanche photodiodes have been used in these applications. In order to obtain an image, scanning of the light source and/or detector is necessary, requiring mechanical components and significantly increasing the acquisition time. As SPAD imagers integrate thousands of pixels, they allow the acquisition of time-resolved images without the need of mechanical components and thus reducing the acquisition time.

In the above mentioned applications it is critical to detect the time of arrival of the photons with the highest possible precision. This may be best achieved in architectures where the detection and time-of-arrival coding is realized in the same integrated circuit. A typical method to code time-of-arrival is based on arrays of time-to-digital converters (TDCs), a circuit similar to a chronometer, but with a timing resolution of the order of picoseconds. To optimize time conversion uniformity, the SPAD is generally placed close to the TDC, possibly a few micrometers away. In the project MEGAFRAME, this was achieved by placing a TDC in every pixel [8].

SPAD detectors' output is binary. In order to increase the intensity resolution, the same detector needs to be read out many times. This may lead to a power and bandwidth problem if the chip has many pixels. One solution to this problem was to include in-pixel analog or digital counters [9, 10] that accumulate the result during a certain period of time.

All the above mentioned solutions require a considerable amount of additional in pixel transistors, thus reducing the fill factor (i.e. sensitive area per total sensor area) and consequently the photon detection efficiency (PDE). A lower PDE results in a much lower signal to noise ratio and therefore in longer acquisition times. Due to the complexity of the systems implemented in pixel for SPAD sensors, often the fill factor shrinks to 1% [8]. Conventional lenses focus the light in a continuous manner that means they can focus light in an area to create an image or a single spot. However in non-continuous detectors, such as imagers with many low fill factor pixels, most of the light hits the inactive area between pixels. An effective way to reclaim some of this lost light is the use of microoptical devices with sizes comparable to the pixel's size. Microconcentrators, such as plano convex microlenses, have been extensively applied in CCD and CMOS sensors [11] to address this problem. Other geometries applied in solar panel technologies have been proposed to recover even more light [12], however so far it is very hard to fabricate them. The main difference between SPAD and CMOS/CCD imagers, is that the

former have much lower fill factor and therefore the implementation of proper microconcentrators is critical. Though recovery factors of $\times 25$ have been reported in detectors where the initial fill factor was particularly low [13], arrays of microlenses with high recovery factor and high uniformity have not been reported for practical sizes.

In the present work, we report on an array of 128×128 plano convex microlenses fabricated on a SPAD array with 5% fill factor and $25\mu\text{m}$ pitch [14]. A single microlens is placed in front of each pixel, focusing the light in the active area. An accurate model for the microlens was conceived, verified by extensive ray-tracing simulations, and validated by measurements. The model was in excellent agreement with the measurements under a wide variety of real-life conditions (f-number, illumination levels, etc.), so as to be a useful tool in the design of future arrays of microlenses.

2. Microlens manufacturing

The microlens arrays were fabricated by CSEM Muttens (Switzerland). A quartz mold was utilized to imprint the microlenses in a sol-gel polymer on top of the SPAD array. The polymer used for the fabrication of the microlenses was ORMOCER[®]. In the manufacturing process the polymer is deposited on top of the imager, the mold is then brought into contact with the polymer and pressure is applied. The polymer is then UV cured and thermally stabilized in an oven. The detector was produced by standard CMOS $0.35\mu\text{m}$ high voltage technology, with a pixel pitch of $25\mu\text{m}$ and a photosensitive area of $6\mu\text{m}$ in diameter, resulting in a fill factor of approximately 5%. A graphical representation of nine pixels is shown in Fig. 1. The microlenses have a radius of curvature of $21.77\mu\text{m}$ and a conic factor $k=1.6$, further geometrical details can be seen in Fig. 1. The microlenses focus the incoming light into the photosensitive area of the pixel. Microlenses of the same mold with different heights were produced in order to assess their performance. Scanning electron microscope (SEM) pictures of sample chips were taken (Fig. 2) to assess the quality of the fabrication process. Profilometry of all samples before bonding were performed to verify the height of the fabricated microlenses. A Tencor[®] profilometer is used to measure the height of the microlenses on six points at the edges of the replicated array. Figure 2 shows a chip with microlenses bonded in a package.

3. Simulator

A ray tracer was implemented in Matlab to study the different microlens parameters and to compare the experimental results with our model. This solution was adopted in order to be able to simulate microlenses with any arbitrary surface. As SPAD imagers are mostly targeted for imaging applications, it was decided to implement a simulator in such a way to include the optical system in which the imager would be ultimately integrated. For this reason, the simulator includes four main optical elements: an object plane, a thin lens that mimics the application's optical system, the microlenses, and the image plane. Thin lenses with different f-number and focal length can be set in order to simulate any given optical setup. It is however also possible to generate collimated light in the simulator that hits the detector with different angles of incidence. The simulator was verified by comparing its results with the ones from a commercial ray tracer (WinLens, Qioptiq, Goettingen, Germany). An optical setup consisting of a thin lens and a circular microlens was simulated with both tools. The results showed good agreement indicating that our simulator is accurate.

The ray's origin points are equidistant in the object plane. From each of these points a specific amount of rays are then generated uniformly covering a predefined solid angle. When one of these rays interacts with a surface (thin lens, microlens, metal wire, etc.) the new trajectory and intensity of the refracted/reflected ray is calculated. The intensity of the detected light is calculated adding the energy of all the rays that hit the photosensitive area of the pixel (Fig. 3).

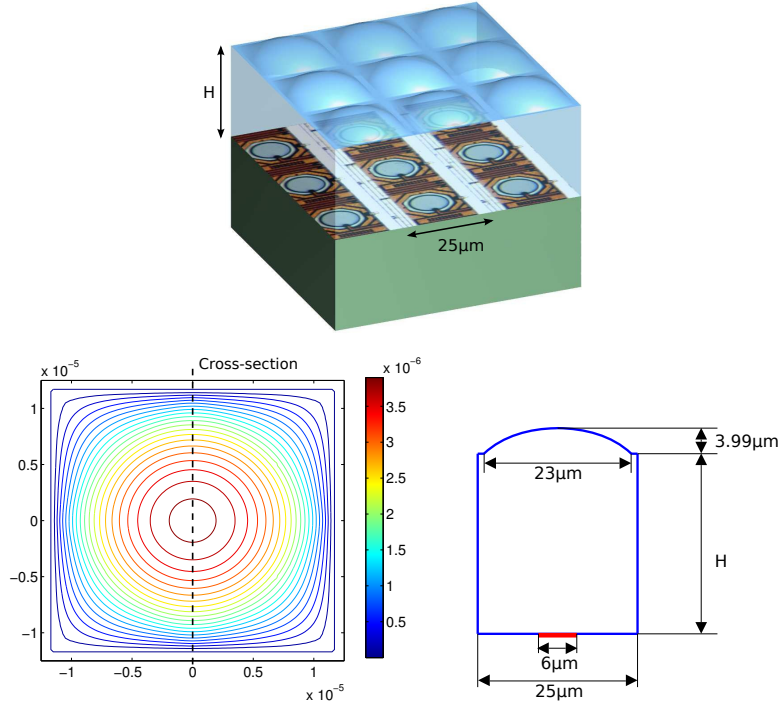


Fig. 1. (top) Detail of array of microlenses mounted on top of nine SPAD pixels. The height of the microlenses H can be adjusted for each sample. (bottom left) Top view of a single microlens with isolines that depict its shape. In this picture it can be seen that the base of the microlens is square, in other words the radius of curvature of the microlenses varies with the azimuthal angle. (bottom right) Cross-section across the dotted line of the microlenses with geometrical details. The active area of the pixel is depicted in red.

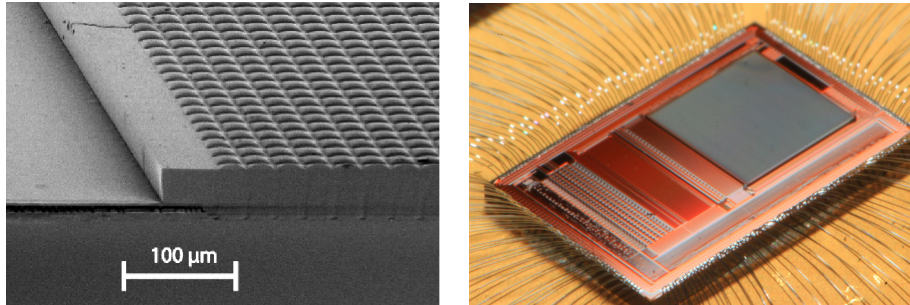


Fig. 2. (left) Scanning electron microscope image of the microlens array fabricated on the CMOS SPAD array. (right) SPAD array chip with microlenses bonded in a PGA package (right).

An array of nine microlenses and nine detectors is simulated to account for optical crosstalk between neighboring microlenses. In order to evaluate the microlenses' performance, we use the concept of concentration factor CF that has been already proposed [12, 13]:

$$CF = E_0/E_i, \quad (1)$$

where E_i is the irradiance (power per unit area) at the input of the microconcentrator, in this particular case the microlens' convex surface, and E_o is the output irradiance of the microconcentrator, that would be the irradiance at the photosensitive area of the pixel. In the current configuration E_i is equivalent to the irradiance that the same photodetector without microlenses would receive. For this reason, the microlenses' concentration factor is obtained by dividing the detected light intensity when microlenses are present by the detected light intensity when the detector has no microlenses.

Since the refractive index of the material used to fabricate the microlenses is quite uniform in the visual spectrum, less than 2.5% difference, and for ease of comparison with previous work [13] which was carried out with white light illumination, the results presented in this work assume a constant refractive index in the microlenses for all wavelengths.

In order to obtain accurate measurements, the discretization error needs to be kept very low, which means that a high number of rays needs to be generated. The simulator has been equipped with Monte Carlo capabilities enabling reliable preliminary results with a reduced number of rays. In this case the distribution of the rays origin points in the object plane is completely randomized, and at each of these points the solid angle is as well randomly sampled.

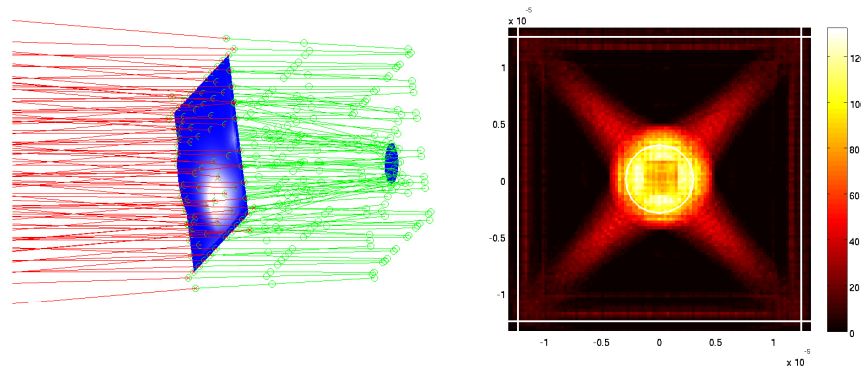


Fig. 3. (left) Ray tracing of light going through a microlens and then reaching the image plane, the circle on the right denotes the photosensitive area of the pixel. Although an array of nine microlenses and nine detectors are simulated, only one microlens and detector are depicted in this figure for clarity purposes. (right) Light intensity profile in the image plane. The outer white straight lines define the limits of the pixel and the inner white circle the pixel's photosensitive area.

4. Results

The concentration factor of microlenses has been tested on the above mentioned 128x128 SPAD array. The initial microlenses were designed for a microscopy application in which the numerical aperture (NA) in the image plane was close to 0.005. The microlenses' calculated back focal-length (BFL) for this particular application was $40\mu\text{m}$. The same microlens mold was applied to produce microlenses of different heights. Several samples were manufactured at a variety of heights. We report in this paper two samples at $30\mu\text{m}$ and $70\mu\text{m}$ height. The height of microlenses is defined as the distance from the base of the microlenses to the photosensitive area in the microchip. Figure 4 shows a SEM cross-section of a diced chip where the height of the microlenses can be measured.

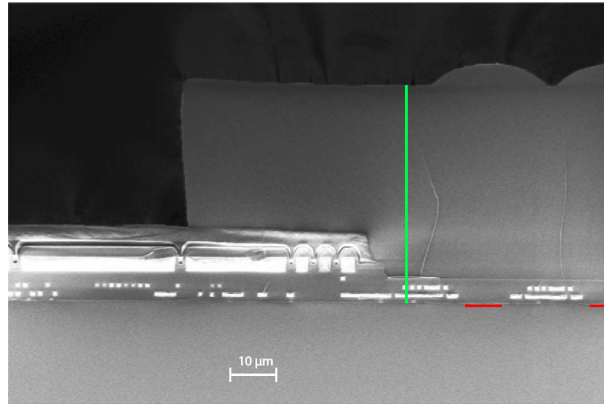


Fig. 4. SEM picture of the cross-section of one of the chips with microlenses. In the array's photosensitive area, marked in red, the upper layers of the microchip have been etched away to increase the performance of the sensor. Metal 1 through 4 are also visible in the cross-section, covered by $2\mu\text{m}$ of SiO_2 passivation and a polyimide layer. The height of the microlenses is marked in green. For this particular sample the height of the microlenses was $51\mu\text{m}$.

All the simulation and experimental results reported in this section were obtained by means of a telecentric objective lens with a magnification factor $\beta = 0.07$. This objective lens is composed of two main elements, a singlet front element (double convex singlet, 200mm focal length, 110mm diameter) and a rear objective lens (15mm focal length, $f/1.4$).

Simulations showed (Fig. 5) that the performance at different f -numbers can be optimized by adjusting the height of the microlenses. As expected for high f -numbers, the optimal performance is achieved when the microlenses' height is similar to the calculated BFL of the microlenses. However for low f -numbers a small height of the microlenses leads to a higher concentration factor. The latter is due to the fact that the concentration factor obtained from skew rays at large apertures is higher than the one obtained from paraxial rays. Figure 5 right shows how the maximum concentration factor for each f -number shifts towards smaller heights as the f -number decreases.

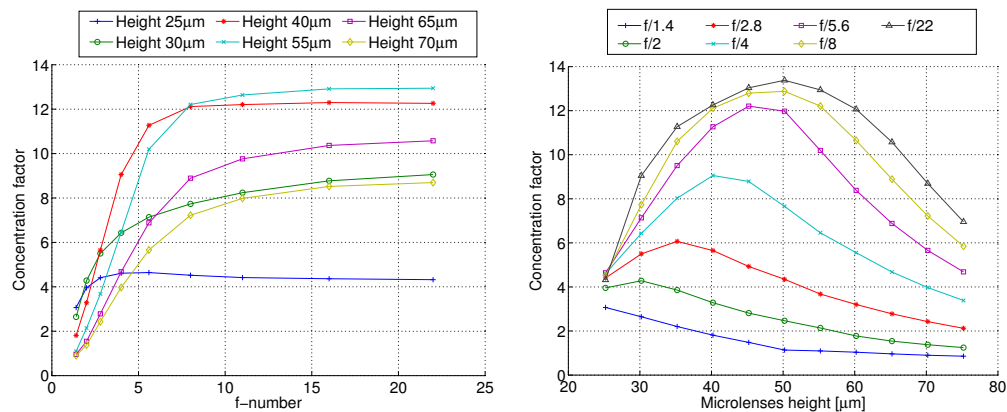


Fig. 5. (left) Simulated concentration factors for different heights of the microlenses. (right) Depending on the application's f -number, the optimal height of the microlenses varies.

The correct height of the microlenses is a key parameter that needs to be controlled in the fabrication process, because it has a tremendous impact in the performance of the sensor. Figure 6 shows substantial concentration factor variations for small height changes. The microlenses' total height depends not only on the height of the sol-gel polymer, but on the different metal and SiO₂ layers that are on top of the photosensitive area of the sensor as well. This means that for an accurate production of the microlenses, the actual height of the different layers in the sensor needs to be measured beforehand. Typically the CMOS process specification state that variations of up to $\pm 2\mu\text{m}$ are possible. Therefore it is important to determine the height of the different layers before the production.

The heights of the different layers were measured in the SEM cross-section (Fig. 4). Since all chips originate from the same wafer we assume that the heights of the different layers were the same for all of them. The total height of the layers related to the CMOS process differed from the specific values by $1\mu\text{m}$. A profilometer was performed on each sample to measure the height of the imprinted microlenses with high accuracy. This value together with the height obtained from the SEM measurement corresponds to the total microlens height of each sample.

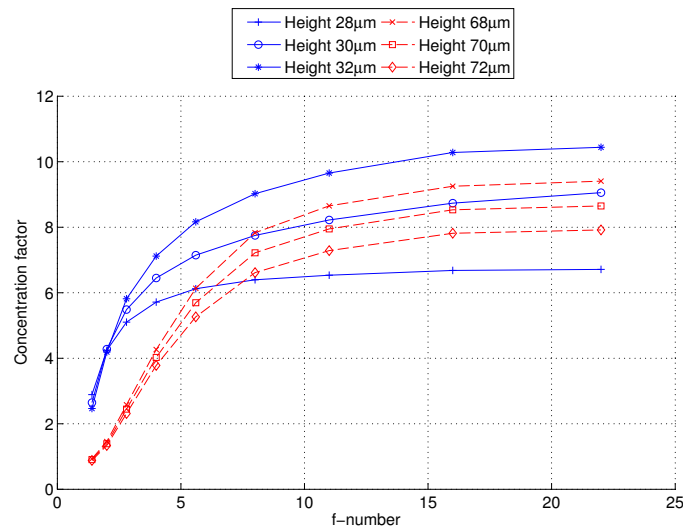


Fig. 6. Concentration factor variations for small height changes.

The concentration factor is empirically computed as the ratio of the average counts in a sensor with and in a sensor without microlenses, using a given primary lens and a well controlled illumination of the scene. To compensate for variations between different chips, the average counts of each sensor are compared using no primary lens and the same diffused light, where microlenses have no effect and cause no concentration. The ratio between the two measured counts is used to correct for any technological differences. Different scenes will result in different average counts, however, the ratio between different sensors should stay the same, as long as no saturation is observed and the majority of pixel counts are above dark count rate (DCR). Experimental measurements showed a good correspondence between samples with and without microlenses. The intensity in the sample with microlenses was approximately 5% lower, which was probably caused by the fact that the diffuse light still had some directivity.

With the above mentioned inter-sample correction factor, measurements were performed on the two samples with $30\mu\text{m}$ and $70\mu\text{m}$ height microlenses, and on another sample without microlenses which served as reference. In the experiments a constant white light source illuminated two targets and then measurements were performed at different f-numbers. The reflecte

light by a white target was measured during the higher f-number measurements in order to have enough signal above the noise level. In the low f-number measurements a black target reflects the light coming from the illumination system so the signal would not saturate the sensor. The concentration factors were experimentally measured on the two samples and then compared with the simulations. Figure 7 shows the median concentration factor of the pixels in each sensor obtained experimentally and the simulated values for each f-number. This comparison showed good agreement.

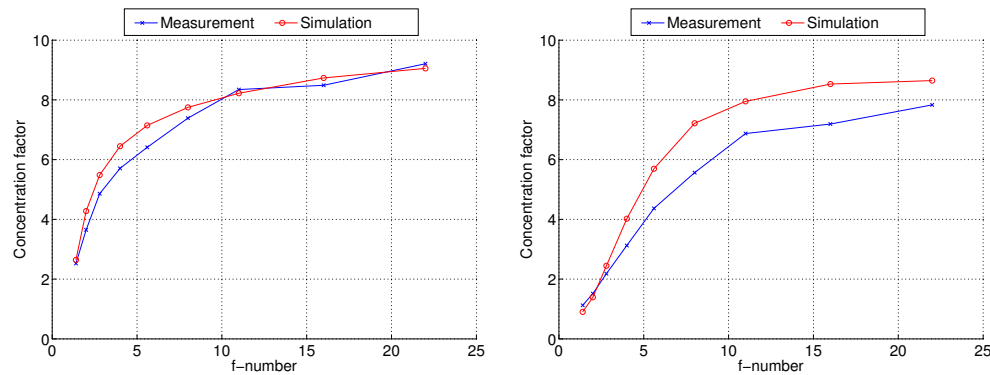


Fig. 7. Concentration factor measurements and simulations of a sensor with 30μm (left) and 70μm (right) height microlenses.

Figure 8 shows images obtained with two SPAD sensors, one with 30μm height microlenses and another one without them. All the images were taken using the same USAF resolution target under the same lighting conditions. The acquisition time for each picture was 200μs, two acquisitions were performed for each sensor, one with the illuminated target and another with the sensor in complete darkness to measure the DCR for each pixel. The DCR value was then subtracted from the picture of the USAF resolution target to enhance the contrast and minimize the effects of the DCR on the concentration factor calculation. Hot pixels, i.e. pixels with unusual high DCR, were discarded and the value at its location was calculated with a median filter. These pixels account for approximately 1% of the total amount of pixels, therefore this filtering process has no visible effect on the quality of the final image. In the pictures the intensity scale of the images was adapted for each f-number to enhance the visibility of the images. The scale of the concentration factor images has been kept constant to facilitate the comparison between them. Here the improvement due to microlenses is clearly visible, specially at high f-numbers. In the images the increase in light intensity is clearly visible when microlenses are used. Moreover, since the main source of noise in SPAD imagers is the DCR, and this is not altered by the microlenses, an increase in intensity due to the microlenses means an increase in signal to noise ratio. This should, however, not be visible in these examples, as they had been compensated for DCR. Nevertheless, it is not always possible in every application to make this compensation and therefore microlenses are generally beneficial to increase signal-to-noise ratio and intensity.

The uniformity of the concentration factor is as well observable in the images of Fig. 8. The concentration factor for each image and its calculated standard deviation are shown in Table 1. The standard deviation is relatively high, compared to previous studies [13]; it is caused mainly by the telecentric error, and it increases with the f-number. For low f-numbers the size of the focal spot is substantially larger than the pixels active area, therefore a small focal spot decentering will have almost no effect on the irradiance within the pixel active area. As the f-

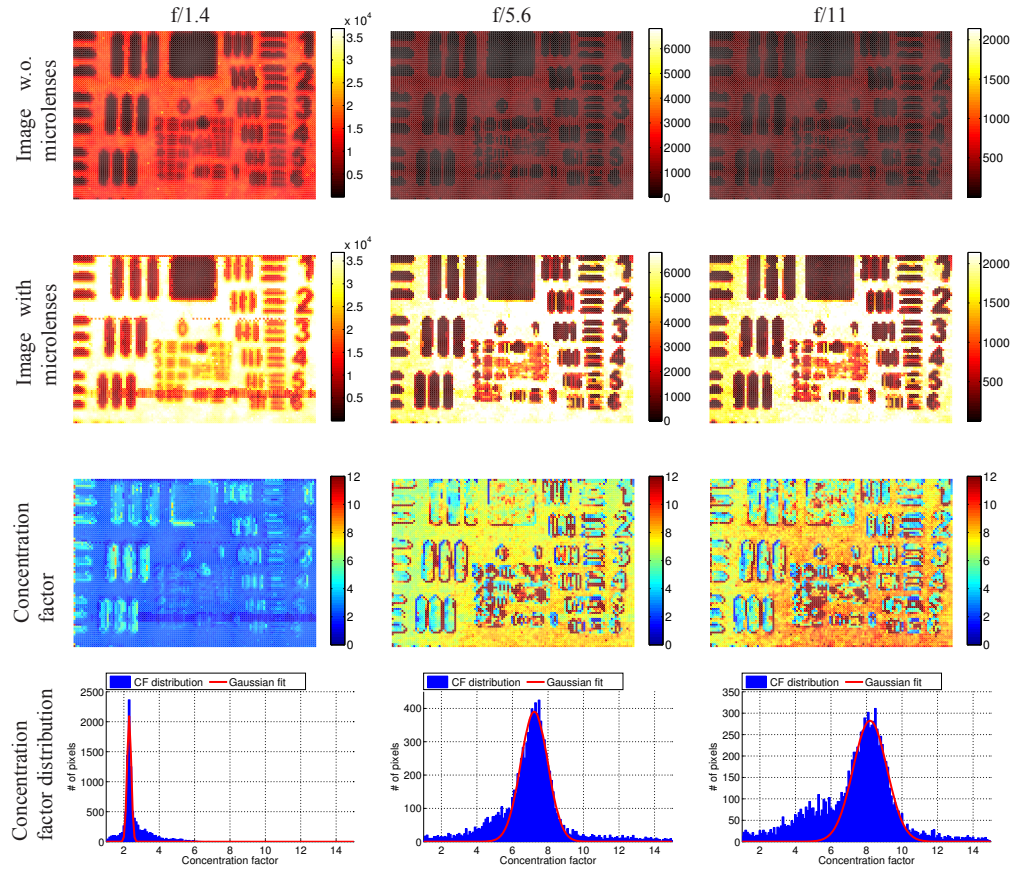


Fig. 8. Image crops obtained from SPAD sensors with $30\mu\text{m}$ height microlenses and without microlenses at different f-numbers. The concentration factor obtained with the microlenses increases at higher f-numbers, and so does its standard deviation.

number increases, the size of the focal spot decreases. When the focal spot reaches a size similar to the pixel active area the centering of the focal spot becomes more critical. In this case a small displacement of the focal spot has a tremendous impact as the irradiance in some parts of the pixel active area drops to almost zero. The microlenses at the center of the image circle receive light rays at an angle that approaches 90 degrees, while periphery microlenses are hit at an angle, as a consequence the focal spot in periphery pixels will be decentered and therefore they will experience reduced concentration factors at high f-numbers. The same effect occurs in case of misalignment between pixels and microlenses. At low f-numbers the focal spot centering is not that critical and therefore the concentration factor will not vary with respect to perfectly aligned microlenses, whereas at high f-numbers a small misalignment between microlenses and detectors can have a big impact in the concentration factor (Fig. 9). This explains the mismatch between the simulations and measurements at high f-numbers presented in Fig. 7 for the $70\mu\text{m}$ sample.

It is important to determine the true value of the height of the microlenses, but it is not always possible to measure it for each sample with profilometries if many of them are fabricated. Nor is desirable to apply a destructive method such as dicing a sample for SEM measurements. In these cases we propose a novel method, i.e. to project angular incident collimated light on the

Table 1. Concentration factor and its standard deviation for different f-numbers.

	f/1.4	f/2.8	f/5.6	f/11	f/22
Concentration factor	2.32	5.34	7.36	8.08	9.34
Standard deviation	0.18	0.30	0.76	0.95	1.70

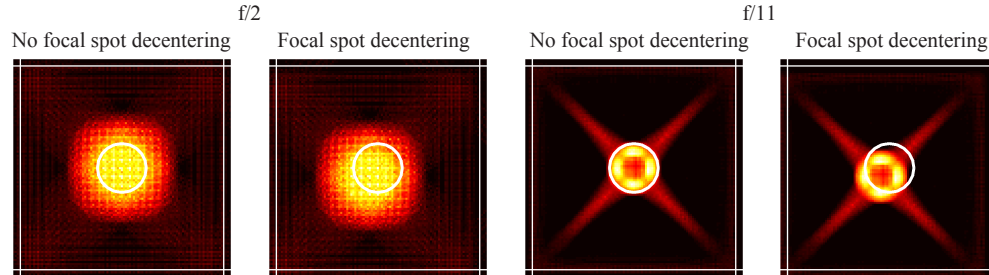


Fig. 9. Light intensity profile in the image plane for $f/2$ and $f/11$ when the focal spot is perfectly centered and in case of focal spot decentering due to microlenses misalignment or telecentric error. For high f-numbers a small focal spot decentering will dramatically reduce the irradiance in certain parts of the pixel active area (enclosed in a white circle). For $f/2$ the concentration factor dropped from 4.3 to 4.0 when the misalignment was introduced, whereas for $f/11$ the concentration factor changed from 8.1 to 6.8. In these simulations microlenses with $30\mu\text{m}$ were used and the focal spot was decentered $1\mu\text{m}$ in the X and Y directions.

sensor, which reveals the exact height of the microlenses. If the microlenses and the detectors are well aligned, the measured intensity will be at a maximum for light incident perpendicularly to the chip. As the polar angle of incidence increases, the focus spot moves away from the photosensitive area and therefore the measured intensity rapidly decreases. At a certain polar angle the focus spot will enter the next neighboring pixel. This angle depends on the design of the microlenses and the height of the imprinted microlenses. Therefore by measuring at which polar angle the peak in intensity appears, it is possible to calculate the height of the microlenses. Figure 10 shows the angle dependency simulations for microlenses of different heights and the experimental measurement performed on one of the sensors. The secondary peak position versus the height of the microlenses is reported in Fig. 11.

In this case there is good agreement between the simulations and the measurements since the microlens array and the sensor were well aligned and no significant gradient in the concentration factor, and therefore in the height of the microlenses, was observed. Measurements at 0° and 90° azimuthal angles were performed to verify that the alignment was correct. In case of a misalignment between the sensor and the microlenses, a complete scanning in polar and azimuthal angles would enable to measure the misalignment and/or tilt of the microlenses and to still determine their height. In case of misalignment between the microlenses and the sensor, the intensity peak would not be at 0° azimuthal and polar angles, but at a different one. By measuring at which polar and azimuthal angles the peak occurs, it is possible to measure the misalignment. If these angles are not constant for all the pixels, that means that there is not only a misalignment but that the microlens array is tilted.

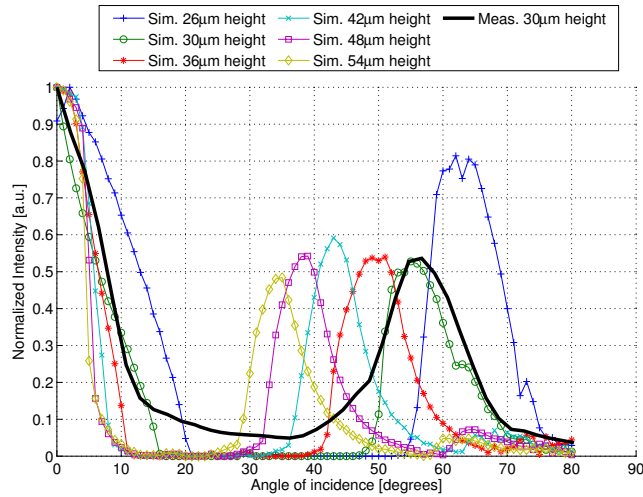


Fig. 10. Light intensity dependence versus angle of incidence for different simulated microlenses heights and measurements obtained from a sensor with $30\mu\text{m}$ height microlenses.

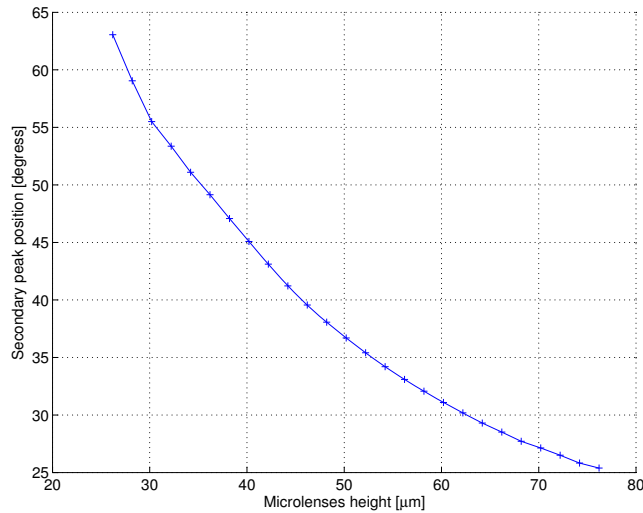


Fig. 11. Secondary peak position variation with respect the microlenses height.

5. Conclusion

We have shown the relation between concentration factor of imprinted microlenses and f-number. We demonstrated that the optimal height of the microlenses depends strongly on the f-number of the whole optical system.

We have developed a reliable simulation software, whose projected values agree well with the experimentally measured values. We also introduced a new contact-less non-destructive method to determine the height of the microlenses, which can be applied in mass production. These results show that microlenses can compensate substantially for very low f-numbers such as for SPAD imagers and enable the development of new microlens designs tailored for each specific application.

Acknowledgments

This work was supported by the KFSP Tumor Oxygenation and the KFSP Molecular Imaging of the University of Zurich.